Proceedings of ASME Turbo Expo 2006
Power for Land, Sea and Air
May 8-11, 2006, Barcelona, Spain

GT2006-91020

INVESTIGATION OF 3D UNSTEADY FLOWS IN A TWO-STAGE SHROUDED AXIAL TURBINE USING STEREOSCOPIC PIV AND FRAP—PART II: KINEMATICS OF SHROUD CAVITY FLOW

Y. I. Yun*, L. Porreca, A. I. Kalfas**, S. J. Song*, R. S. Abhari****
* School of Mechanical and Aerospace Engineering, Seoul National University, Seoul, Korea
** Turbomachinery Laboratory, Swiss Federal Institute of Technology Zurich, Zurich, Switzerland

ABSTRACT

This paper presents an experimental study of the behavior of leakage flow across shrouded turbine blades. Stereoscopic particle image velocimetry and fast response aerodynamic probe measurements have been conducted in a low-speed two-stage axial turbine with a partial shroud. The dominant flow feature within the exit cavity is the radially outward motion of the main flow into the shroud cavity. The radial migration of the main flow is induced by flow separation at the trailing edge of the shroud due to a sudden area expansion. The radially outward motion is the strongest at mid-pitch as a result of interactions between vortices formed within the cavity. The main flow entering the exit cavity divides into two streams. One stream moves upstream towards the adjacent seal knife and reenters the main flow stream. The other stream moves downstream due to the interaction with the thin seal leakage flow layer. Closer to the casing wall, the flow interacts with the underturned seal leakage flow and gains swirl. Eventually, axial vorticity is generated due to these complex flow interactions. This vorticity is generated by a vortex tilting mechanism and gives rise to additional secondary flow. Due to these fluid motions combined with a contoured casing wall, three layers (the seal leakage layer, cavity flow layer, and main flow) are formed downstream of the shroud cavity. This result is different from the two-layer structure which is found downstream of conventional shroud cavities. The seal leakage jet formed through the seal clearance still exists at 25.6 percent axial chord downstream of the second rotor. This delay of complete dissipation of the seal leakage jet and its mixing with the cavity flow layer is due to the contoured casing wall. Time-averaged flow downstream of the shroud cavity shows the upstream stator's influence on the cavity flow. The time-averaged main flow can be viewed as a wake flow induced by the upstream stator whose separation at the shroud trailing edge induces pitchwise non-uniformity of the cavity flow.

INTRODUCTION

Shrouds are used to prevent pressure-driven leakage flow across the turbine blade tip. Nevertheless, there is still a gap between the stationary (casing wall or stator shroud) and rotating parts (rotor shroud or stator hub), and flow leaks through the gap. To reduce the leakage flow, labyrinth seals are often employed. Much work has been done to clarify how the labyrinth seal affects flow field not only within the seal cavity but also downstream of the blade passage. To quantify loss with a simple model, Denton [1] made a simplified description of the cavity flow that the meridional velocity of the leakage jet undergoes dissipation inside the shroud cavity while the swirl of the leakage flow remains unchanged. Thus, there is a mismatch of flow angle between the leakage and the main flows when the two flows interact. The mismatch causes a shear layer which is a source of loss [1, 2]. According to Wallis et al. [3], a strategy for reducing the losses associated with seal leakage flow is to minimize the entropy generated during the interaction between the seal leakage and the main flow. They added airfoil shaped turning devices on top of the shroud surfaces to turn the leakage flow through the shroud cavity, but actually found performance degradation. Also, the seal leakage flow causes negative incidence on the subsequent stator, thus intensifying the passage vortex formed inside the subsequent stator [4-6]. Song and Song [7] developed an analytical model to predict flow response to labyrinth seals in an axial turbine stage with a shrouded rotor. In their control volume approach, they assumed that the leakage flow is radially inward at the exit of the cavity and the leakage and the main flows remain separate downstream. Thus, downstream of the shroud cavity, there are two flow layers—the main flow and the leakage flow which is retarded in the axial direction and tangentially underturned.

It was not until recently that the flow within the seal cavity was experimentally investigated in detail. Pfau et al. [8] made detailed measurements of the flow within the shroud cavity in an annular turbine cascade. They found a pitchwise variation in static pressure within the shroud cavity as well as radially outward and inward motions of fluid at the exit cavity. They inferred that the pitchwise non-uniformity of the flow within the cavity is attenuated as the leakage flow passes through three seal knives, presumably due to the mixing in the cavities. Also, they observed a radially stratified axial velocity distribution and a toroidal vortex within the exit cavity. Pfau et al. [9]

investigated the flow field at the inlet of the shroud cavity in a rotating turbine rig, and found that the interaction between the main flow and cavity flow is mainly driven by a toroidal vortex moving at 83 percent of the rotor speed. Pfau et al. [10] also proposed nonaxisymmetric contouring on the shroud surface to reduce the leakage flow based on detailed flow measurements within the shroud cavity. Wolter et al. [11] conducted time-resolved flow field measurements within three seal cavities formed by two seal knives attached to the shrouded turbine rotor blades. They observed, in the first cavity, a pitchwise non-uniformity due to the leading edge potential effect, which was also observed by Pfau et al. [8]. Furthermore, they found that the flow became tangentially uniform as it passed through the second cavity, and then regained non-uniformity due to the interaction with the main flow in the exit cavity.

Conventional shroud covering the rotor blades extends beyond both the leading edge and trailing edge of the rotor blades in the axial direction. This type of full shroud increases the inertia near the rotor tip region, and, consequently, rotor blades may suffer from structural problems. Porreca et al. [12] investigated the effects of partial shroud on turbine aerodynamics. The partial shroud covers less than 40 percent of the axial chord of the rotor and aims to reduce inertia as well as leakage. According to Porreca et al. [12], the underturned flow extends from the casing down to 60 percent and 80 percent span regions in the partial shroud case and full shroud case, respectively. They attributed the difference to the pressure driven leakage flow through the tip clearance of the shroudless trailing edge region of the partially shrouded blades.

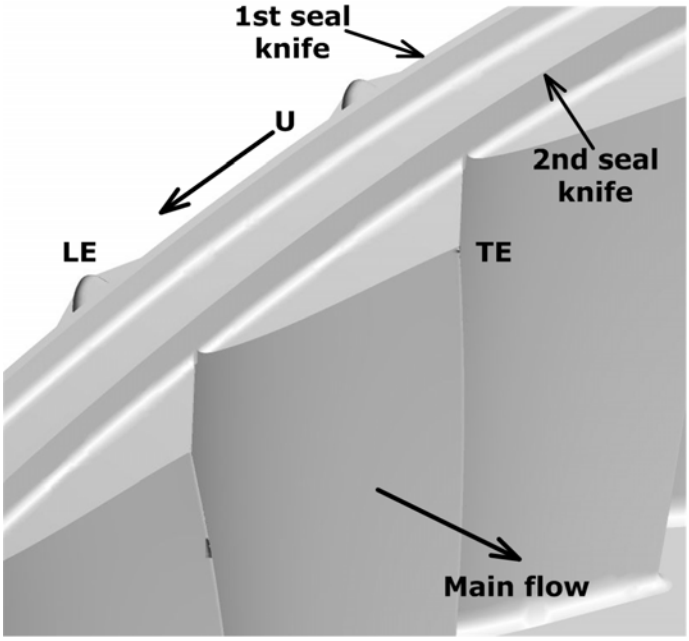

Figure 1 Partially shrouded rotor

Though much work has been done on the nature of seal leakage flows in classical shroud cavities ([7-11]), little is known about the detailed kinematics of the cavity flow in partially shrouded turbines and its interaction with the main flow. This second part of the two-part paper presents an experimental study of shroud cavity flow in a two-stage shrouded axial turbine test facility. The partial shroud geometry has been modified as shown in Fig. 1. Shroud is added near the pressure side at the trailing edge to inhibit the pressure-driven leakage flow over the blade tip, which was observed by Porreca et al. [12]. The main focus of this paper is on the exit cavity flow behavior.

Stereoscopic particle image velocimetry (PIV) technology has primarily been used for this investigation. By using PIV, detailed flow field has been observed on several blade-to-blade measurement planes in the shroud exit of the second rotor. PIV is useful for this investigation because it is possible to observe not only the flow in the shroud cavity region but also the streamwise evolution of flow with fine spatial resolution. Also, unsteady pressure measurements have been carried out in an axial plane downstream of the second rotor by using fast response aerodynamic probe (FRAP) technology developed at Swiss Federal Institute of Technology Zurich [13, 14].

The objective of this study is to address the following questions by observing the time-averaged as well as phase-locked averaged flow field in the turbine.

- How does the leakage flow behave within the partial shroud exit cavity?
- What are the major flow features in the interaction between the leakage and main flows in a partially shrouded turbine?
- How does the seal leakage flow evolve downstream of the shroud cavity combined with a contoured casing wall?
- In the fixed frame downstream of the shroud cavity, how does each of the upstream stator and the rotor's geometry affect the shroud cavity flow?

DESCRIPTION OF THE EXPERIMENT

Test turbine rig

The present study has been conducted in a low speed, quasi-closed loop, 2-stage axial turbine rig at Swiss Federal Institute of Technology Zurich in Switzerland. All measurements have been carried out at the design condition. Table 1 summarizes the design parameters of this turbine facility. More detailed desciptions of the facility and its operation can be found in Porreca et al [15].

Rotating speed	2625 rpm
Pressure ratio	1.38
Mass flow rate	10.65 kg/s
Number of Blades (Stator / Rotor)	42 / 42
Aspect ratio	1.8
Tip diameter	800 mm
Mach Number (Stator / Rotor)	0.35 / 0.1
Reynold Number	2×10^5

Table 1 Design parameters of the test turbine

Instrumentation

Two measurement techniques—stereoscopic PIV and fast response aerodynamic probe (FRAP)— have been used for the

present investigation. The test turbine is equipped with a transparent optical window, which extends from -78 to 103 percent axial chord from the trailing edge of the second rotor and 1.2 blade pitch to facilitate an optical access to the shroud cavity region. The casing ring is rotatable for azimuthal traversing of aerodynamic probes such as FRAP.

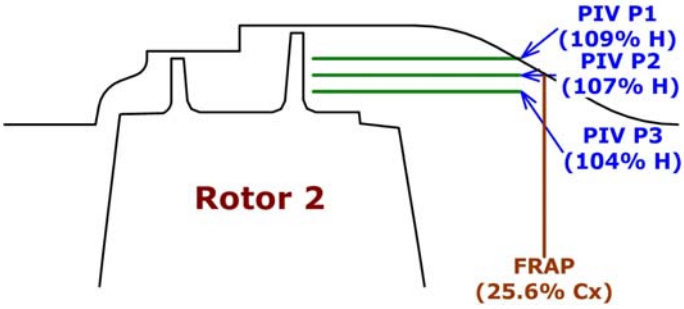

Figure 2 Measurement planes within the cavity and downstream of the second rotor

Figure 2 shows PIV and FRAP measurement planes within the cavity and downstream of the second rotor. Stereoscopic PIV has been conducted in three radial planes within the shroud cavity—P1, P2, and P3 at 109, 107, and 104 percent span, respectively. One blade passing period has been divided into 10 time steps, and 100 image pairs have been recorded in each plane at each time step. FRAP measurement has been made in an axial plane located at 25.6 percent axial chord from the trailing edge of the second rotor. The FRAP measurement grid comprises 1502 points distributed uniformly—32 points in the circumferential direction (3.5 percent pitch in 1.1 pitch) and 47 points in the radial direction. More detailed descriptions of both measurement techniques can be found in Porreca et al [15].

The measurement uncertainty of stereoscopic PIV has been estimated by conducting a Monte Carlo simulation. Monte Carlo simulation has proven to be effective to evaluate PIV error because one can prescribe parameters such as particle diameters, number of particles, displacement vectors, etc [16]. To carry out the simulation, tracer particle images are artificially generated by assuming that the light intensity scattered from individual particles has a Gaussian profile. The initial location of each tracer particle is set by using a random number generator and the locations of displaced particles in the second image frame are determined with predefined displacement vectors. After calculating cross-correlation with these images, one can obtain artificially generated PIV results, compare them against the predefined velocity values, and estimate PIV errors. Detailed descriptions of the simulation can be found in Yun [17].

300 image pairs have been generated for several points within the shroud cavity to carry out statistical evaluations. PIV error consists of *bias error* and *random error* [16]. Bias error is defined as the difference between the mean PIV value and the actual value. Random error is the standard deviation of the PIV values and is regarded as measurement uncertainty. Figure 3 shows PIV errors estimated at a typical point within the cavity for 100 image pairs and 300 image pairs. The errors for each velocity component have been normalized by the actual values for each component. The errors from 100 image pairs are comparable to those from 300 image pairs. Therefore, 100 image pairs have been used. The bias errors of tangential and axial velocities are about 2~3 percent while that of radial velocity is about 17 percent. The actual value of tangential velocity is slightly outside the uncertainty range, and that of axial velocity lies within the uncertainty range. The uncertainty levels of both velocities are about 2~6 percent. The actual value of radial velocity is outside the uncertainty range of about 12 percent. The error in radial velocity (or out-of-plane velocity) is larger than those of in-plane components (tangential and axial velocities) and this trend is consistent with the results reported in previous research [18]. Although the PIV error in radial velocity is larger than those of conventional probes, important flow features can still be captured.

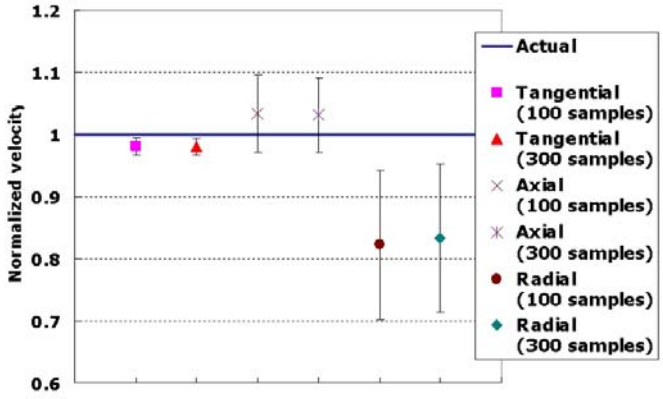

Figure 3 PIV errors at a typical measurement point within the cavity

RESULTS AND DISCUSSION

The aim of this investigation is to clarify the kinematics of the flow within the shroud cavity of the second rotor. The flow features downstream of the second rotor are then examined.

Time and Pitchwise Averaged Features of the Cavity Flow

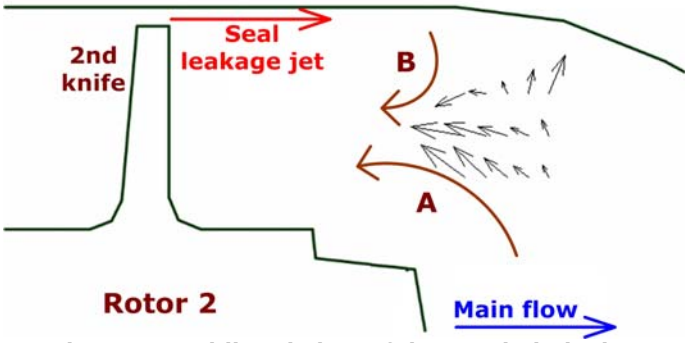

Figure 4 Meridional view of time and pitchwise averaged velocity within the cavity

Figure 4 shows the meridional view of time and pitchwise averaged velocity field within the cavity. Signals could not be

obtained above the shroud surface due to the reflection of the laser light. Therefore, time and pitchwise average was taken in the region downstream of the trailing edge of the shroud. The most prominent feature found within the cavity is the radially outward and axially backward fluid motion. The fluid exiting the blade passage migrates radially outward into the shroud cavity and moves upstream toward the second seal knife (indicated as 'A' in Fig. 4). At the upstream edge of the measured area near the casing, the fluid motion is radially inward and axially backward ('B' in Fig. 4). This motion originates from flow separation at the tip of the second seal knife. At the downstream edge of the measured area near the casing, the fluid resumes forward motion due to the interaction with the seal leakage flow. Though the seal leakage flow is not clearly captured because the measurement plane closest to the casing wall is 4 mm away from the wall, it can be hypothesized that there exists a thin seal leakage layer above the measurement region adjacent to the casing wall.

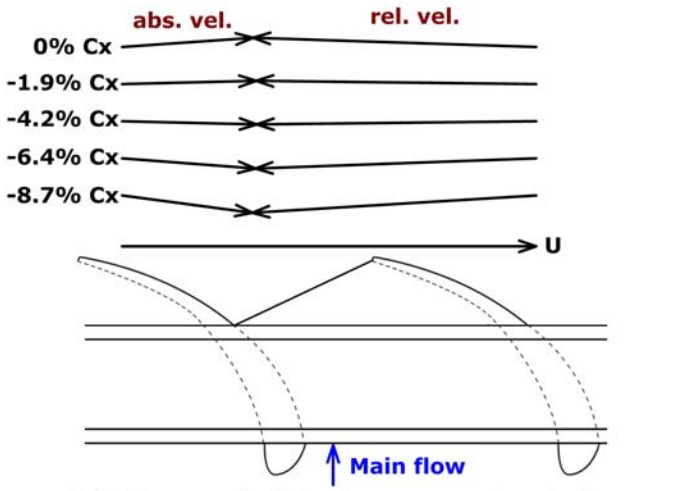

(a) Time- and pitchwise averaged velocity triangles at 109 % span at different axial locations

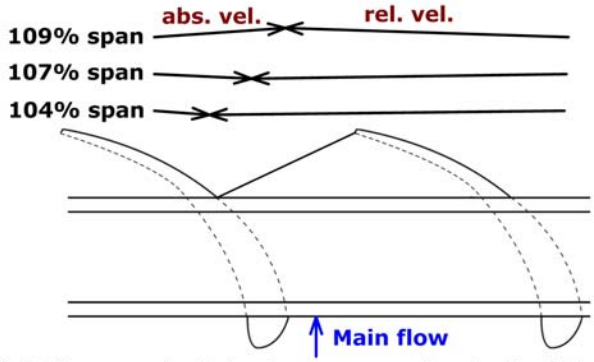

(b) Time- and pitchwise averaged velocity triangles at different radial locations at the blade TE (0% Cx)

Figure 5 Time and pitchwise averaged velocity triangles within the cavity

Velocity triangles show time and pitchwise averaged azimuthal flow features. Figure 5 (a) shows the axial evolution of velocity triangles in the uppermost measurement plane within the cavity (109 percent span). The flow gains positive axial momentum as it moves downstream. Absolute tangential velocities show underturned behavior and the swirl level remains the same toward downstream. This underturning is due to the interaction of the cavity flow with the seal leakage flow.

Figure 5 (b) shows velocity triangles of the cavity flow at three different spanwise locations at 0 percent axial chord from the trailing edge of the rotor. The flow closest to the main passage is still influenced by the radially outward and axially backward moving main flow with little swirl. However, the flow gains positive axial momentum and swirl due to the interaction with the seal leakage flow as it approaches the casing wall.

Upstream Stator Effect

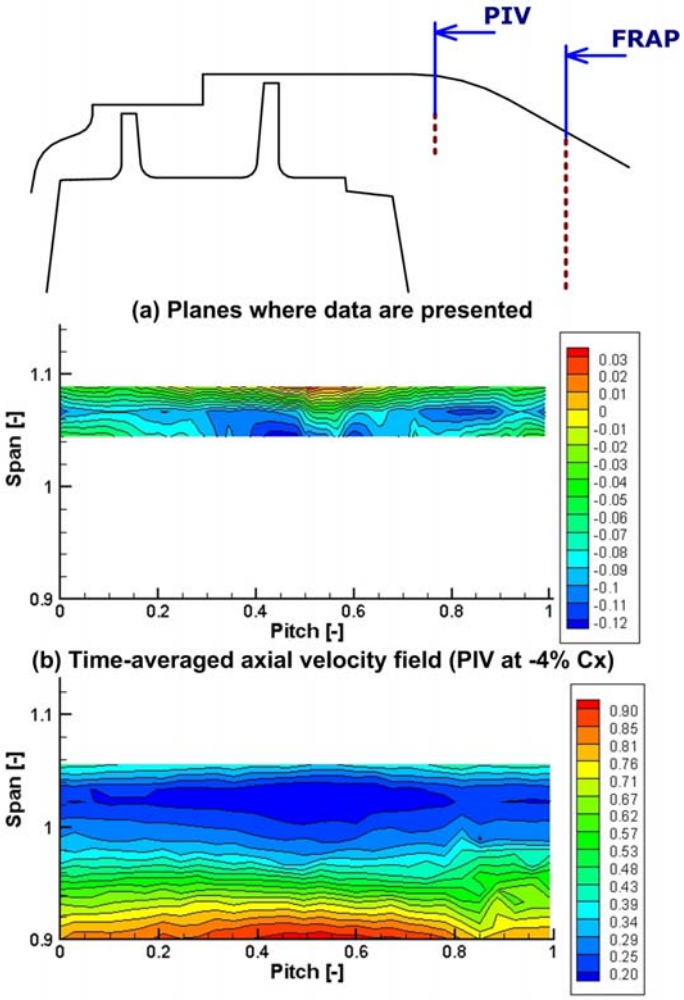

(a) Planes where data are presented

(b) Time-averaged axial velocity field (PIV at -4% Cx)

(c) Time-averaged axial velocity field (FRAP at 25.6% Cx)

Figure 6 Time-averaged axial velocity fields within and downstream of the cavity

Figure 6 (a) shows the axial locations— -4 percent axial chord and 25.6 percent axial chord— where PIV and FRAP were respectively used to obtain time-averaged axial velocity fields. In the PIV measurement, the blade passing period has

been divided into 10 time steps, and the time average has been taken with 10 phase-locked averaged data sets. With FRAP, the time average has been taken with 109 phase-locked averaged data sets for a blade passing period.

In the cavity (measured with PIV and shown in Fig. 6 (b)), the reversed flow is still dominant. The seal leakage jet with positive axial velocity appears near the casing wall. Also, a pitchwise variation of the time-averaged axial velocity is visible, and the reversed flow is the strongest at mid-pitch. The pitchwise variation indicates the upstream stator's influence on the cavity flow for the following reason. The measurements of both PIV and FRAP have been done in the fixed frame, and time-averaging filters out the pitchwise variation due to the motion of the rotor. Thus, a pitchwise variation of parameters in the time-averaged results can be attributed only to fixed frame disturbances such as the upstream stator.

At 25.6 percent axial chord downstream, no reversed flow is observed any more (Fig. 6 (c)). Spanwise variation of axial velocity is similar to that within the cavity. The lowest axial velocity lies between 100 and 104 percent span. This indicates that the spanwise variation originates from the three layers near the shroud cavity—seal leakage jet, reversed cavity flow due to separation, and the main flow. Also, at 90 percent span, a pitchwise variation of the main flow is observed. The pitchwise location of the maximum velocity (0.5 pitch) of the main flow coincides with that of the minimum velocity of the cavity flow. The reason for this coincidence is explained later.

Effect of Partial Shroud Geometry

Figure 7 shows the pitchwise velocity profiles immediately downstream of the blade trailing edge within the cavity. The location where the data have been obtained is indicated in Fig. 7 (a). The location has been selected because the data there show the most prominent pitchwise variation. The data elsewhere show similar though weaker patterns. Pitchwise variations of normalized radial and axial velocities are plotted in Figs. 7 (b) and (c), respectively. The velocities have been normalized by the axial velocity obtained by dividing the mass flow rate by the annulus area and density. Each velocity profile is a phase-locked average of 100 instantaneous data at each time step. In each plot, velocity profiles at five different time steps (t/T=0.2, 0.4, 0.6, 0.8, 1) have been plotted versus the rotor blade pitch. Due to relative motion between the optical window and the rotor, the location of measurement region relative to the rotor blade is different for each time step. Therefore, the velocity data in Fig. 8 have been adjusted so that their relative position to the rotor blade is the same. Overall, the velocity data collapse into one curve showing pitchwise variations of radial and axial velocities. These pitchwise variations are due to the shape of the partial shroud and rotate with the rotor.

In Fig. 7 (b), the strongest radially outward motion of the main flow occurs at mid-pitch. The radially outward motion decays closer to the blades, and the flow becomes radially inward near the blades. Also the cavity flow has zero axial velocity at the mid-pitch location and negative axial velocity near the blades (Fig. 7 (c)). The pitchwise profile of the axial velocity has the same phase as the radial velocity.

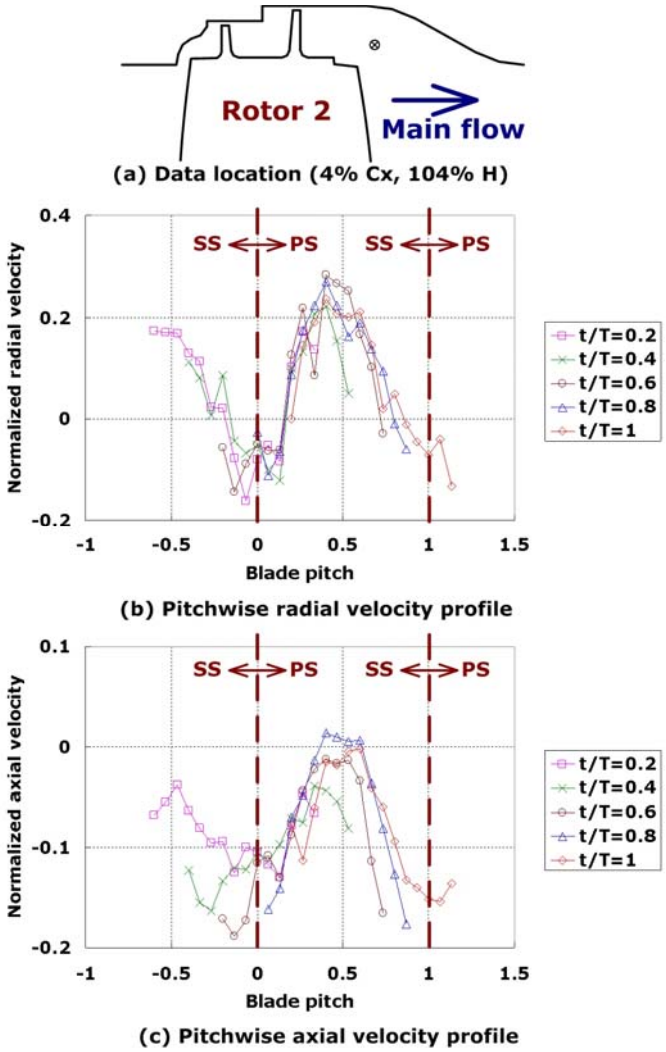

Figure 7 Pitchwise velocity profiles downstream of the blade trailing edge within the cavity

These flow patterns can be understood better by examining velocity field in meridional planes. Figure 8 shows the velocity fields in 5 meridional planes in one pitch within the cavity. Near the blades (Figs. 8 (b) and (f)), the flow pattern is radially inward and axially backward. This pattern is nothing more than vortical motion 'B' (Fig. 4) which originates from flow separation at the tip of the seal knife. Near mid-pitch (Figs. 8 (c), (d), and (e)), radially outward and axially backward motion (motion 'A' in Fig. 4) is dominant within the cavity. Above the measured region, it can be hypothesized that motion 'B' exists there but is located near the casing and the seal knife. Overall, motion 'B' moves back and forth at a fixed tangential location while the blade rotates. Near the blades, motion 'A', which is weaker than the case at mid-pitch, does not appear. These motions of two vortical structures (motions 'A' and 'B') can be explained in terms of vortex interactions shown in Fig. 9.

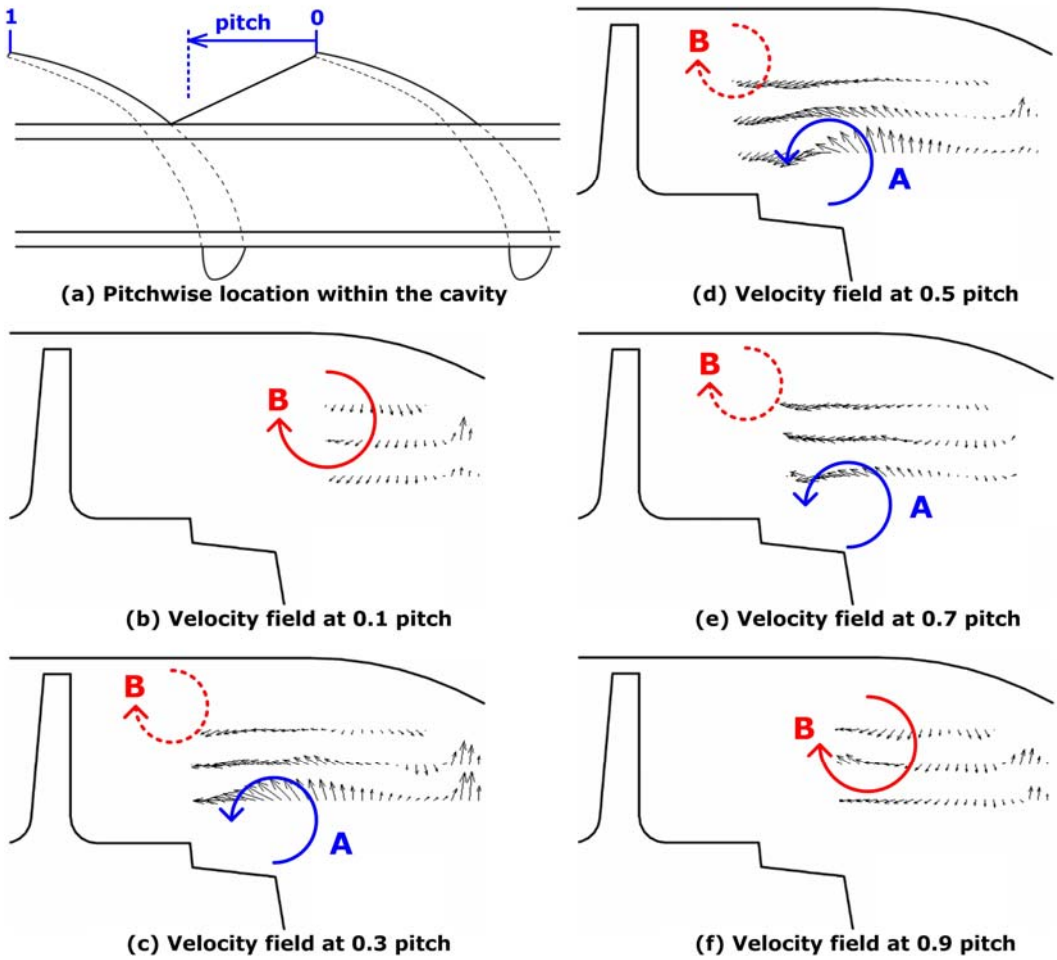

Figure 8 Meridional velocity fields within the cavity

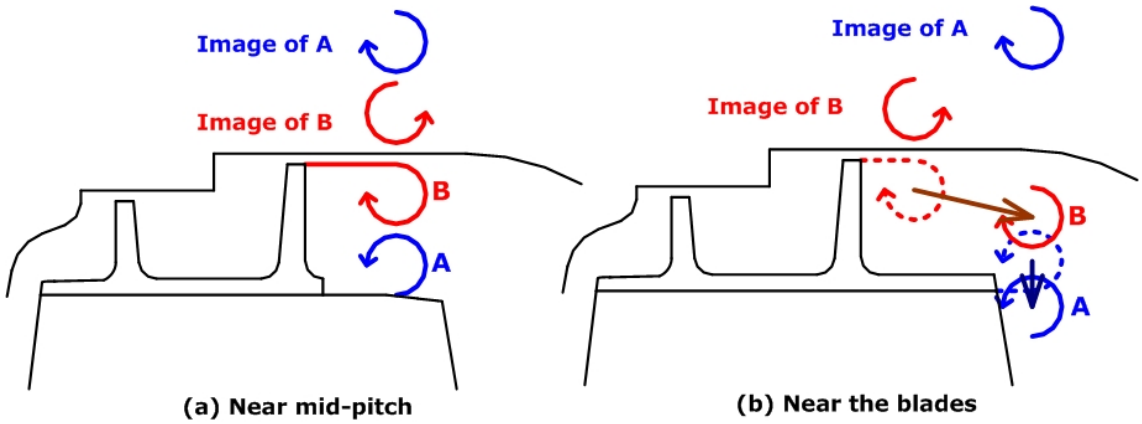

Figure 9 Vortex interactions within the cavity

Below the inner surface of the shroud, the main flow exits the main passage while there is a dead flow zone above the outer surface of the shroud. Thus, the main flow is subject to a sudden area expansion and separates at the shroud trailing edge. The separated flow rolls up into vortex 'A'. Due to the similar reason, the seal leakage flow separates at the tip of the seal knife and turns into vortex 'B'. Both vortices affect each other (Fig. 9). Near mid-pitch (Fig. 9 (a)), vortex 'B' stays close to the adjacent seal knife due to the force induced by vortex 'A'. The centers of each vortex are almost axially aligned so that a radial velocity on vortex 'A' induced by other vortices is small. Near the blades, however, the axial extension of the shroud reaches the blade trailing edge. Thus, vortex 'A' is located farther downstream than vortex 'B'. In this case, the axially

backward motion of 'B' induced by 'A' is much weaker than the axially forward motion induced by the image vortex of 'B'. Therefore, vortex 'B' moves farther downstream than at mid-pitch. Also, a radially inward velocity on 'A' is induced by vortex 'B' since the axial locations of both vortices are not aligned. Thus, vortex 'A' is weakened or absent near the blades since vortex 'B' suppresses the flow separation at the shroud trailing edge.

For this reason, the strongest radially outward motion of the flow takes place near mid-pitch (Fig. 7 (b)). Also, near mid-pitch in Fig. 7 (a), the radially outward motion with little axial motion due to vortex 'A' is dominant. However, at the same location near the blades, the axially backward motion due to vortex 'B' is prevalent. Thus, the pattern in Fig. 7 (c) can be explained.

Generation of Axial Vorticity Within the Shroud Exit Cavity

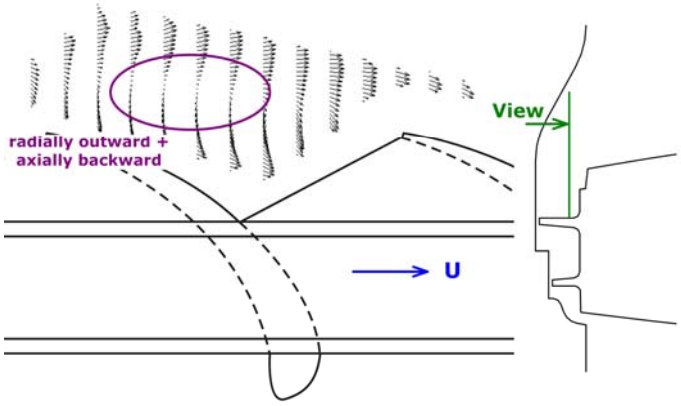

(a) Absolute velocity field in P3 (104 % span, t/T = 0.8)

(b) Absolute velocity field in P2 (107 % span, t/T = 0.8)

Figure 10 Absolute velocity fields on blade-to-blade planes within the cavity

In reality, fluid particles within the cavity do not move two-dimensionally (as shown in Fig. 8) but three-dimensionally. The path of fluid particles in 'A' (Fig. 8) can be inferred by examining the absolute velocity fields in radial planes within the cavity (Fig. 10). Fig. 10 (a) and (b) show the phase-locked averaged velocity fields in the planes at 104 and 107 percent span, respectively, at a time step t/T=0.8. The data at t/T=0.8 have been chosen because the entire blade passage is visible through the optical window at this time step. Only the velocity data 4 mm apart from each other in the circumferential direction have been shown to enhance visibility. Fluid particles move radially outward and axially backward with little swirl in the plane at 104 percent span (encircled zone in Fig. 10 (a)). Fig. 10 (b) shows that these particles gain swirl as they approach the casing wall by interacting with the underturned seal leakage flow and this motion corresponds to vortex 'A' (Fig. 8). Downstream, fluid particles moving radially outward also gain swirl due to the interaction with the seal leakage flow and then move downstream.

These three-dimensional flow features can be explained in terms of vorticity kinematics and an order of magnitude analysis. The axial, azimuthal, and radial directions are denoted by x_1, x_2, and x_3, respectively (Fig. 11). According to the PIV data in Fig. 10, the length scale along which the flow varies in the x_3 direction is much smaller than those in the x_1 and x_2 directions. The length scale in the x_1 and x_2 directions is approximately the blade pitch while that in the x_3 direction is the shear layer thickness which is formed within the cavity as

$$\begin{matrix} x_1, x_2 \sim L \\ x_3 \sim \delta \end{matrix} \quad \text{where} \quad \delta << L \tag{1}$$

Furthermore, the characteristic velocity in the x_1 and x_2 directions is the rotating speed.

$$u_1, u_2 \sim U \tag{2}$$

Thus, the orders of magnitude of each vorticity component can be estimated.

$$\begin{matrix} \omega_1, \omega_2 \sim \dfrac{U}{\delta} \\ \omega_3 \sim \dfrac{U}{L} \end{matrix} \tag{3}$$

The flows in the current investigation can be assumed to be incompressible because the Mach number at the exit of the rotor is 0.1 (Table 1). Thus, baroclinic effects can be neglected. Also, the flow has been observed in the fixed frame so that non-conservative forces such as Coriolis force can be neglected. Therefore, the vorticity equation is as follows.

$$\frac{D\omega_i}{Dt} = \omega_j \frac{\partial u_i}{\partial x_j} + \nu \frac{\partial^2 \omega_i}{\partial x_j \partial x_j} \tag{4}$$

where i=1, 2, 3.

With Eq. (3), the order of magnitude of each term of vorticity equation can be evaluated. Here, only the axial and tangential vorticity components (i=1, 2) are considered. The magnitude of the first term (tilting and stretching term) on the right hand side in Eq. (4) is approximately

$$\omega_j \frac{\partial u_i}{\partial x_j} \sim \frac{U^2}{\delta L} \tag{5}$$

The magnitude of the second term (viscous term) on the right hand side in Eq. (4) is

$$\nu \frac{\partial^2 \omega_i}{\partial x_1^2}, \nu \frac{\partial^2 \omega_i}{\partial x_2^2} \sim \frac{1}{\mathrm{Re}} \frac{U^2}{\delta L} \tag{6}$$

$$\nu \frac{\partial^2 \omega_i}{\partial x_3^2} \sim \frac{1}{\mathrm{Re}} \frac{U^2}{\delta L} \left(\frac{L}{\delta} \right)^2 \tag{7}$$

The viscous terms in Eq. (6) is smaller than the tilting and stretching term Eq. (5) by a factor of 1/Re. In the current study, the Reynolds number is of an order of 10^5. Thus, Eq. (6) can be neglected compared to Eq. (5). The viscous term in Eq. (7) is larger than Eq. (6) by a factor of $(L/\delta)^2$. In the current case, $(L/\delta)^2 \sim 10^2$, and Eq. (7) is still three orders of magnitude smaller than Eq. (5). Thus, the viscous effects can be neglected and the vorticity field within the cavity is mainly dominated by tilting or stretching.

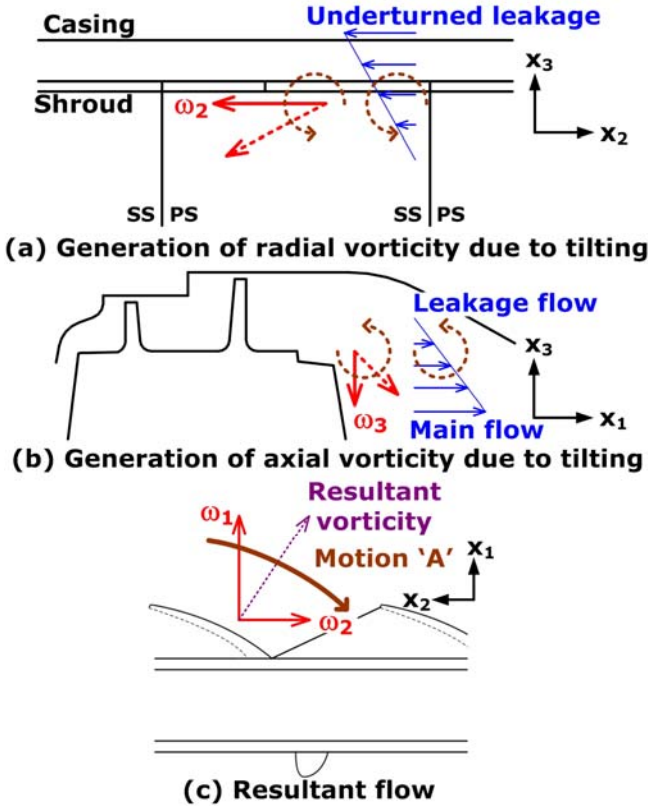

Figure 11 Vorticity kinematics of the exit cavity flow

Figure 11 shows the main vortical features within the shroud cavity. As displayed in Fig. 9, flow separation due to a sudden area expansion gives rise to motion 'A' near mid-pitch. This motion has a tangential vorticity component. As shown in Fig. 11 (a), there is a radial gradient of tangential velocity between the underturned leakage flow and the main flow. If the vorticity is slightly tilted due to a perturbation such that it has a radial vorticity component, the radial vorticity becomes negative due to the tangential velocity gradient. In a meridional view (Fig. 11 (b)), there is a radial gradient of axial velocity between the main flow and the axially retarded leakage flow. This velocity gradient tilts the negative radial vorticity such that a positive axial vorticity is generated. The resultant vorticity is shown in an azimuthal view (Fig. 11 (c)). The vorticity has three components (the radial component is not shown in the figure) and the velocity field induced by this vorticity is consistent with motion 'A' shown in Fig. 10. The generation of axial vorticity gives rise to additional secondary flow downstream of the rotor, and, eventually, increases loss.

Downstream Flow Features

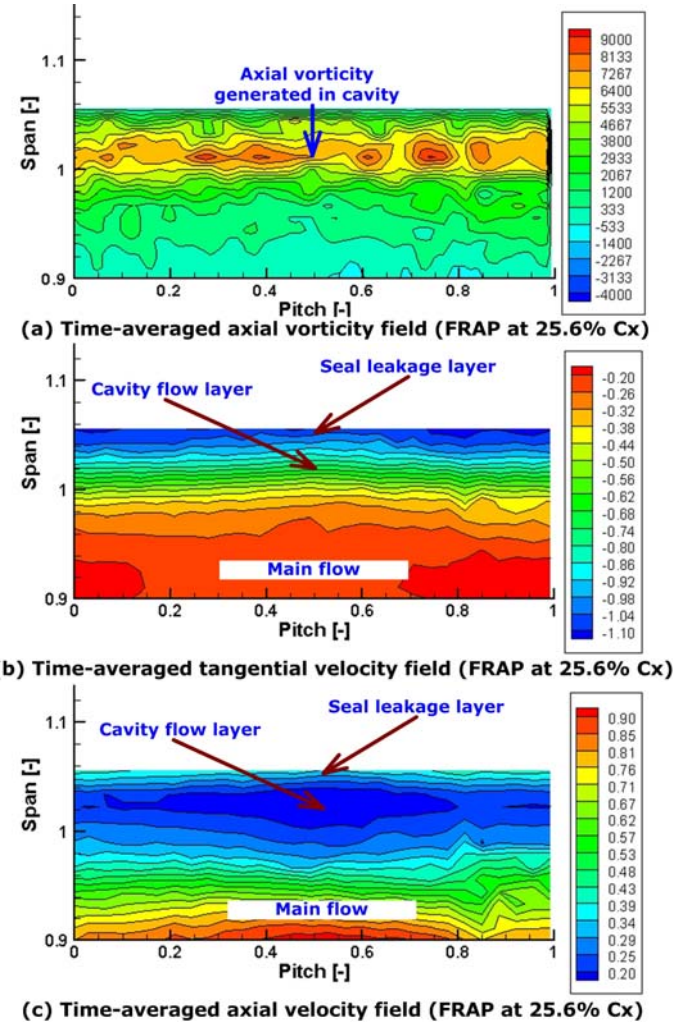

Figure 12 Time-averaged flow velocities downstream of the shroud cavity

The axial vorticity discussed in the previous section can be observed farther downstream of the shroud cavity. Figure 12 shows time-averaged axial vorticity, axial and absolute tangential velocity fields at 25.6 percent axial chord

downstream of the second rotor. The flow parameters have been obtained with FRAP. Between 100 percent and 102 percent span, there exists axial vorticity which originates from the flow within the cavity (Fig. 12 (a)). Though this axial vorticity will eventually enhance mixing between the main flow and the seal leakage flow, there is still a clear division between the seal leakage layer and the main flow at this axial location. Between those two streams, there is a layer with different axial and tangential velocities from those of the leakage and main flows (termed cavity flow layer in Fig. 12). This feature is not clearly discernible in the tangential velocity field (Fig. 12 (b)), where the seal leakage layer closest to the casing wall has the strongest swirl and the swirl gradually becomes weaker away from the casing wall. However, in the axial velocity field (Fig. 12 (c)), the cavity flow layer, with the lowest axial velocity, between the main flow and the seal leakage layer is visible.

In classical shroud configurations (full shrouds and the casing wall recessed at 90°), the seal leakage jet is known to be dissipated inside the cavity before it exits the cavity [1]. Thus, it is commonly assumed that the flow downstream of such cavity has two layers—the seal leakage layer and main flow [7]. However, in the current investigation with a partial shroud and a contoured casing wall, the seal leakage jet remains at 25.6 percent axial chord downstream of the second rotor. The delay of dissipation is due to the contoured casing wall because it prevents direct impingement of the jet onto the cavity wall at the exit of the cavity and reduces the interaction of the leakage flow with the main flow [19].

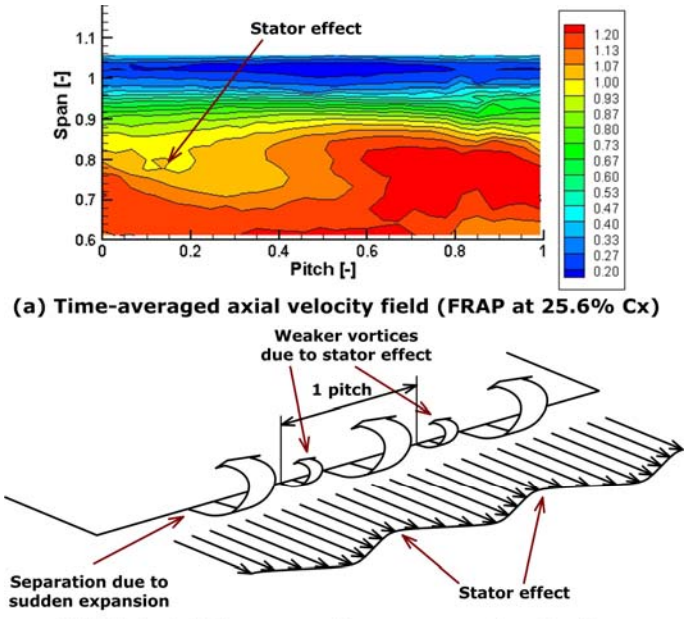

(a) Time-averaged axial velocity field (FRAP at 25.6% Cx)

(b) Stator's influence on time-averaged cavity flow

Figure 13 Upstream stator effect on time-averaged cavity flow

Figure 13 presents an explanation for the coincidence between loci of the minimum axial velocity in the cavity layer and the maximum axial velocity of the main flow (Fig. 6). Figure 13 (a) shows the time-averaged axial velocity field in the fixed frame in the same axial plane as that in Fig. 6 (c) but covering a larger spanwise region. The axial momentum defect due to the upstream stator (wake and secondary flow) is visible at 80 percent span and this can be simplified as a wake flow induced by the upstream stator. At the exit of the second rotor passage, the wake flow meets a sudden area expansion and separates. The flow with momentum defect rolls up into a weaker vortex whereas that with higher momentum induces a stronger vortex (Fig. 13 (b)). Thus, the pitchwise variation in the time-averaged cavity flow originates from the wake flow due to the upstream stator. The time-averaged flow field downstream of the second rotor can be simplified as a wake flow passing through a splitter plate (rotor shroud) above which no axial flow exists. Above the no axial flow zone closer to the casing wall, the seal leakage jet (not displayed in Fig. 13 (b)) exists.

CONCLUSIONS

Detailed flow field measurements have been carried out within and downstream of the exit shroud cavity in an axial, two-stage, partially shrouded turbine with a contoured casing wall. New conclusions from this investigation are as follows:

1. In the exit cavity, the radially outward motion of the main flow into the shroud cavity is the dominant flow feature. The radial migration of the main flow is induced by flow separation at the trailing edge of the shroud due to a sudden area increase.
2. The main flow entering the exit cavity divides into two streams. One stream moves upstream towards the adjacent seal knife and reenters the main flow stream. The other stream moves downstream due to the interaction with the thin seal leakage flow layer. Fluid particles in both streams are entrained by the underturned seal leakage flow as they approach the casing wall, and thus gain swirl.
3. Due to the interaction between the vortex shed at the shroud trailing edge ('A') and the vortex shed at the tip of the adjacent seal knife ('B'), the radially outward and axially backward motion is the strongest near mid-pitch while motion 'B' is dominant within the cavity near the blades.
4. The vortical flow structures within the cavity are inviscid and vorticity generation is mainly determined by vortex tilting. Due to this tilting mechanism, axial vorticity is generated within the cavity. The generation of axial vorticity gives rise to additional secondary flow downstream of the rotor, and, eventually, increases loss.
5. At 25.6 percent axial chord downstream of the second rotor, three layers - the seal leakage layer, cavity flow layer, and main flow – are distinctly visible. The seal leakage jet layer still exists at 25.6 percent axial chord downstream of the second rotor. The delay in the dissipation of the jet is due to the contoured casing wall.
6. Time-averaged flow feature downstream of the shroud cavity shows the upstream stator's influence on the cavity flow. The time-averaged main flow through the second rotor can be simplified as a wake flow which separates at the shroud trailing edge. This separation induces a pitchwise non-uniformity of the cavity flow layer.

ACKNOWLEDGMENTS

The authors gratefully acknowledge Alstom Power Switzerland for their kind permission to publish the results. Mr. Y. I. Yun gratefully acknowledges support from the BK21 Project of the Korea Ministry of Education & Human Resources Development and Professor R. S. Abhari of the Swiss Federal Institute of Technology Zurich, Switzerland. He would also like to thank Dr. T. Kim at Xian Jiaotong University, China, for his helpful comments.

NOMENCLATURE

C_x	axial chord length of the rotor blade
H	rotor blade span
L	blade pitch
LE	leading edge
PS	pressure side
Re	Reynolds number
SS	suction side
t	time
T	a blade passing period
TE	trailing edge
U	rotor speed
u	velocity
x	spatial variable
δ	shear layer thickness
ν	kinematic viscosity
ω	vorticity

Subscripts

1	tangential direction
2	axial direction
3	radial direction

REFERENCES

[1] Denton, J.D., 1993, "Loss Mechanisms in Turbomachines—the 1993 IGTI scholar lecture", ASME J. Turbomachinery, **115**(4), pp. 621-656.

[2] Hunter, S.D., and Manwaring, S.R., 2000, "Endwall Cavity Flow Effects on Gaspath Aerodynamics in an Axial Flow Turbine: Part I – Experimental and Numerical Investigation," ASME Paper No. 2001-GT-651.

[3] Wallis, A.M., Denton, J.D., and Demargne, A.A.J., 2001, "The Control of Shroud Leakage Flows to Reduce Aerodynamic Losses in a Low Aspect Ratio, Shrouded Axial Flow Turbine", ASME J. Turbomachinery, **123**(2), pp. 334-341.

[4] Peters, P., Breisig, V., Giboni, A., Lerner, C., and Pfost, H., 2000, "The Influence of the Clearance of Shrouded Rotor Blades on the Development of the Flowfield and Losses in the Subsequent Stator", ASME Paper No. 2000-GT-478.

[5] Giboni, A., Menter, J.R., Peters, P., Wolter, K., Pfost, H., and Breisig, V., 2003, "Interaction of Labyrinth Seal Leakage Flow and Main Flow in an Axial Turbine", ASME Paper No. GT2003-38722.

[6] Giboni, A., Wolter, K., Menter, J.R., and Pfost, H., 2004, "Experimental and Numerical Investigation into the Unsteady Interaction of Labyrinth Seal Leakage Flow and Main Flow in a 1.5-Stage Axial Turbine", ASME Paper No. GT2004-53024.

[7] Song, B.H., and Song, S.J., 2004, "Lateral Forces from Single Gland Rotor Labyrinth Seals in Turbines", ASME J. Eng. Gas Turbine & Power, **126**(3), pp. 626-634.

[8] Pfau, A., Treiber, M., Sell, M., and Gyarmathy, G., 2001, "Flow Interaction from the Exit Cavity of an Axial Turbine Blade Row Labyrinth Seal", ASME J. Turbomachinery, **123**(2), pp. 342-352.

[9] Pfau, A., Schlienger, J., Rusch, D., Kalfas, A.I., and Abhari, R.S., 2005, "Unsteady Flow Interactions within the Inlet Cavity of a Turbine Rotor Tip Labyrinth Seal", ASME J. Turbomachinery, **127**(4), pp. 679-688.

[10] Pfau, A., Kalfas, A.I., and Abhari, R.S., 2004, "Making Use of Labyrinth Interaction Flow", ASME Paper No. GT2004-53797.

[11] Wolter, K., Peters, P., Giboni, A., Menter, J.R., and Pfost, H., 2005, "Experimental and Numerical Investigation of the Unsteady Leakage Flow Through the Rotor Tip Labyrinth of a 1.5-Stage Axial Turbine", ASME Paper No. GT2005-68156.

[12] Porreca, L., Behr, T., Schlienger, J., Kalfas, A.I., Abhari, R.S., Ehrhard, and J., Janke, E., 2005, "Fluid Dynamics and Performance of Partially and Fully Shrouded Axial Turbines", ASME J. Turbomachinery, **127**(4), pp. 668-678.

[13] Porreca, L., Hollenstein, M., Kalfas, A.I., and Abhari, R.S., 2005, "Turbulence Measurements and Analysis in a Multi-Stage Axial Turbine", 17th Internation Symposium on Airbreathing Engines, September 4-9, 2005, Munich, Germany.

[14] Porreca, L., 2006, "Aerothermal Optimization of Partially Shrouded Axial Turbines", Ph. D. Thesis, Swiss Federal Institute of Technology, Zurich, Switzerland.

[15] Porreca, L., Yun, Y.I., Kalfas, A.I., Song, S.J., and Abhari, R.S., 2006, "Investigation of 3D Unsteady Flows in a Two-Stage Shrouded Axial Turbine Using Stereoscopic PIV and FRAP—Part I: Interstage Flow Interactions", ASME Paper No. GT2006-90752.

[16] Raffel, M., Willert, C.E., and Kompenhans, J., 1998, *Particle Image Velocimetry—a Practical Guide*, Springer-Verlag, Berlin, Germany.

[17] Yun, Y.I., 2006, "Axial Vorticity in the Cavity of a Partially Shrouded Axial Turbine", Ph. D. Thesis, Seoul National University, Seoul, Korea.

[18] Lawson, N.J., and Wu, J., 1997, "Three-Dimensional Particle Image Velocimetry: Error Analysis of Stereoscopic Techniques," Meas. Sci. Technol., **8**(8), pp. 894-900.

[19] Schlienger, J., Pfau, A., Kalfas, A.I., and Abhari, R.S., 2003, "Effects of Labyrinth Seal Variation on Multistage Axial Turbine Flow", ASME Paper No. GT2003-38270.

